Investigations on potential methods for the long-term monitoring of the state of fuel elements in dry storage casks

Hampel, U.; Kratzsch, A.; Rachamin, R.; Wagner, M.; Schmidt, S.; Fiß, D.; Reinicke, S.;

Originally published:

December 2018

Kerntechnik 83(2018)6, 513-522

DOI: https://doi.org/10.3139/124.110949

Untersuchungen zu potenziellen Methoden für die Langzeitüberwachung von Brennelementen in Trockenlagercontainern

Investigations on potential methods for the long-term monitoring of the state of fuel elements in dry storage casks

Uwe Hampel [1,2], Alexander Kratzsch [3], Reuven Rachamin [1], Michael Wagner [1], Sebastian Schmidt [3], Daniel Fiß [3], Sebastian Reinicke [3]

[1] *AREVA Endowed Chair of Imaging Techniques in Energy and Process Engineering, Technische Universität Dresden, 01062 Dresden, Germany*

[2] *Helmholtz-Zentrum Dresden-Rossendorf, 01328 Dresden, Germany*

[3] *Institute of Process Technology, Process Automation and Measuring Technology, Zittau/Görlitz University of Applied Sciences, 02763 Zittau, Germany*

Abstrakt

Mit der verlängerten Zwischenlagerung von abgebrannten Brennelementen ergeben sich verschiedene regulatorische und sicherheitstechnische Fragestellungen. Eine davon ist die nach der Langzeitintegrität der Brennelemente in den Behältern. Ihre Beantwortung hat direkte Relevanz für den späteren Transport zum Endlager und die Umladung des abgebrannten Kernbrennstoffs in andere Behälter. Im Rahmen des vom BMWi geförderten Vorhabens DCS-MONITOR untersuchen wir Potenziale und Grenzen von nichtintrusiven Verfahren zur Überwachung des Zustands des radioaktiven Inventars von Trockenlagerbehältern. Als solche betrachten wir die Thermographie, strahlungsbasierte Messverfahren sowie akustische Messverfahren. Für diese erfolgt eine Bewertung der Empfindlichkeit und Nachweisgrenzen, vorzugsweise durch Nutzung numerischer Simulationen aber auch ausgewählter Experimente.

Abstract

Extended dry storage of spent nuclear fuel is a relevant issue in many countries operating nuclear power plants. Beside regulatory and security aspects there are questions with respect to the long-term integrity of the spent fuel as this is of relevance for final transportation and reloading to final waste repository casks. Within the frame of the BMWi project DCS-MONITOR, we investigate the potentials of different methods for non-intrusive monitoring of dry cask storage containers with spent nuclear fuel. These are thermography, radiation-based methods, and acoustic methods. For all of them we study the sensitivity and cross-sensitivity with respect to defined changes in the nuclear fuel distribution inside the containers. The analyses are mainly based on numerical simulations but also include some dedicated experimental studies.

1. Introduction

Until deep geological disposal for highly radioactive waste is available, it is necessary to safely store spent fuel in intermediate storages on the nuclear power plant site. In Germany, for instance, it is expected that this can be so for periods longer than 50 years. This raises questions about the status of the spent fuel after such a long time. Intermediate storage is in dry storage containers, in Germany of the type CASTOR (Gesellschaft für Nuklear-Service mbH Essen), i.e. CASTOR V/19 for PWR fuel and CASTOR V/52 for BWR fuel. Momentarily, there is a lack of knowledge about the long-term behavior of the cladding material of fuel rods and hence the integrity of this barrier under extended dry storage conditions. Constant production of gaseous decay products over time increase the internal rod pressure, though not all of this gas is released from the fuel matrix. Constant fuel temperature decrease increases the brittleness of the cladding material. Hydrogen embrittlement as well as material degradation during power plant operation, such as fretting and oxidation, make a reliable prediction of long-term fuel element integrity difficult. Therefore, a non-invasive method to detect changes in the cask inventory during extended storage would be highly valuable. However, the massive construction of the storage containers with a 47 cm thick steel wall make such diagnostics very challenging and give way to only very few applicable methods. Before we go into a discussion about such methods in the next chapters, we will briefly review the potential damage mechanisms that give raise to concerns about the cask inventory.

During reactor operation and dry storage the following essential changes or damages in the fuel pellets and fuel rods might occur:

- fretting (reactor operation),
- pellet-cladding-interaction (PCI) (reactor operation),
- corrosion-induced wall weakening (reactor operation),
- hydride intercalation and re-orientation (reactor operation and dry storage),
- creep (dry storage).

Mechanical interactions between fuel rods and spacers of the fuel elements during reactor operation can lead to local mechanical wear, and thus to the weakening of the wall thicknesses (fretting) [1]. Such interactions are caused by flow forces of the coolant. During the reactor operation, the temperatures inside the fuel pellets are about up to 1400 °C and decrease in the direction of the outer pellet areas to about 500 °C. Thereby, the resulting thermal stress leads to a fragmentation of fuel pellets. Due to the fragmentation the outer diameter of the fuel pellets increases. In the case of low internal pressures, the cladding tube material might simultaneously creep inwards (first operating cycles) due to high temperatures (about 320 °C) and high coolant pressure (about 70 – 150 bar under PWR conditions). Consequently, the gap between fuel pellets and the inner cladding tube decreases and the so-called pellet-cladding interaction begins [2, 3]. Subsequent power increases can lead to thermal expansions of the pellets and thus increase the pellet diameter. This, in turn, leads to increased mechanical stresses on the cladding tube material, which can lead to failure of fuel rods during the reactor operation and release of fission products into the primary cooling circuit. In the case of simultaneously occurring corrosion-related processes during the pellet-cladding interaction, the occurrence of fuel rod failure can be intensified. The corrosion-

induced wall weakening of fuel rod cladding tubes during the reactor operation results from the reaction

$$Zr + 2\ H_2O \rightarrow ZrO_2 + 2\ H_2 \quad (1)$$

of the coolant (H_2O) with the zircaloy (Zr) of the fuel rod cladding tube [1]. The reaction results inter alia in the forming of zirconium oxide (ZrO_2), which acts as a protective layer against further corrosion of the cladding tubes. Under PWR conditions (coolant temperatures of about 300 – 320 °C) a closed oxide layer around the cladding tubes can be formed. These oxide layers are a limiting criterion for the application time of the fuel rods or fuel elements. It is assumed that with oxide layer thicknesses of about 150 µm the integrity of the fuel rod cladding is compromised. Furthermore, due to the reaction of coolant (H_2O) with the zircaloy (Zr) of the fuel rod cladding tubes hydrogen (H_2) is being formed as well. During reactor operation, it is absorbed atomically into the crystal lattice of the cladding tube material (hydride intercalation) [5, 6]. The proportion of hydrogen absorbed in the PWR cladding tubes is approximately 8 % to 15 %. The absorbed hydrogen is either dissolved in the crystal lattice or it is present as precipitation in the form of hydride platelets after exceeding the solubility concentration. These hydride dispersions preferably occur near the outer and colder surfaces of the fuel rod cladding tube and are precipitated in a circumferential-oriented form. The mechanical properties of the fuel rod cladding can be adversely affected by the hydride intercalation with simultaneous unfavorable operating conditions.

During the dry intermediate storage, the pressures inside the fuel rods are much higher than the pressures inside the transport and storage casks. Therefore, a higher radial stress gradient for the cladding tubes occurs. Additionally, the radial stress gradient will be favored due to increasing temperatures. Due to the high radial stress gradient, the hydride dispersions which are aligned in a circumferential direction of the cladding tubes during reactor operation and also further hydrides which are settling due to cooling will get a radial direction (re-orientation). Thus, so called radial hydrides are created. These radial hydrides influence the properties in a negative way (hydrogen embrittlement). This could be a reason that the cladding tubes fail by an internal pressure increase [5]. Due to the high temperatures of the fuel elements during the dry intermediate storage the cladding tube material can suffer an irreversible radial wall expansion (creep) [1]. This process favors the weakening of the cladding tube stability.

All of the phenomena discussed above cause a weakening of the cladding material already during operation or later during dry storage. As a result, severely damaged fuel rods may rupture during dry storage. The probability of fuel rods rupture is further increased by high internal pressures and temperatures (primarily in time ranges after the beginning of dry storage). With this in mind the following potential states of the inventory of dry storage containers can be defined:

1. fuel rod cladding rupture
2. relocation of fuel within fuel rods
3. relocation of fuel into the basket
4. relocation of fuel into lower container areas

2. Thermography

The idea of thermography as monitoring method is to use the decay heat as a signal carrier. It is expected that changes of the inventory result in a local change of the temperature distribution on the outer cask wall. For investigating the suitability of this approach, the thermal processes inside and outside the cask have to be modeled including conduction, convection, and radiation. FEM and CFD simulation are used to investigate the sensitivity of the temperature distribution to the geometrical changes of the inventory. There are several challenges that come with thermographic monitoring. Firstly, this approach is an ill-posed inverse problem. Small measurement uncertainties may result in the misleading identification of the inventory state. Further, different inventory states may cause nearly identical temperature distributions. The second problematic issue is the decreasing heat decay. At the beginning of storage, the heating power of spent fuel is up to 39 kW which leads to a temperature of around 75 °C at the outer wall. Decay heat calculations, which were performed for a discharged "Vor-Konvoi"-type German PWR fuel assembly (discharged burnup of 57 GWd/t) using the FISPACT-II code [7], show that after 60 years, the heating power is only 6 % to 15 % compared to the beginning of the storage. In Fig. 1, the average temperature of the outer cask wall over time based on these decay heat calculations is shown. The temperature decreases exponentially. After 60 years of storage the difference between averaged cask wall temperature and ambient air temperature is around 4 K, after 120 years around 2 K. These low differences complicate the identification of temperature gradients on the cask wall. The third challenge is the complex geometry. Within the large CASTOR, relatively thin blades and small gaps of the basket may have a significant influence on the thermal transport processes. Thermal studies for other casks showed that the convection has to be taken into account since it has a significant influence on the heat propagation. Especially, the convection processes in the gap between fuel assembly basket and cask wall may strongly influence the absolute temperature as well as the gradient on the wall [5]. Because of the complex geometry of the cask, CFD simulations of the convection are performed in simplified geometries. In Fig. 1, the temperature distribution of a vertical cut of a simplified CASTOR model is shown. This model includes the simulation of the inner and outer convection. The basket and fuel assemblies are modeled as a homogenous heating element. This simulation provides information about the temperature gradient on the outer cask wall and the natural convection around the cask and between cask wall and basket. Based on such simulations it is possible to extract heat transfer coefficients. In combination with thermal correlations, these results are used as boundary conditions for thermal FEM in more detailed geometries without simulating the complete convection process inside the cask, as this would exceed the computational resources.

For validating the simulation models, the simulation results will be compared with measurements data obtained from an experimental rig. A view of the experimental rig is given in Fig. 2. The main component of the experimental rig is a scaled (1:7.4) CASTOR V/19 container mock-up with an integrated basket model and 19 controllable heating elements (P_{max} = 19 × 100 W). To obtain temperatures of the inner container wall 60 resistance thermometers are placed 1.0 mm from the inner wall inside boreholes. With this, especially the convective processes inside the container will be investigated. Temperatures outside the container can be measured with a number of thermocouples and a thermography camera. The

data will be used for the improvement of the simulation models, and for further development of the thermography method. The experimental investigations are at a preliminary stage.

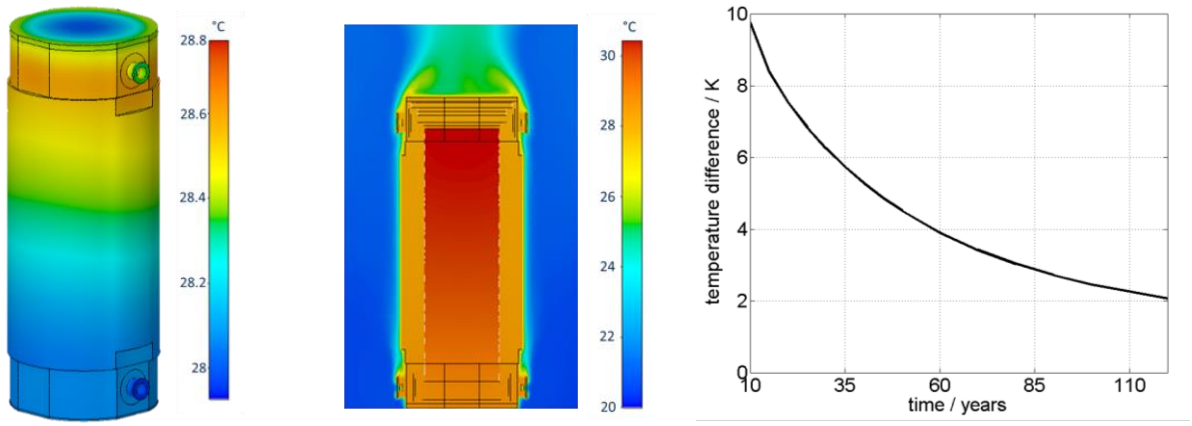

Fig. 1. Left: Simulated temperature distribution on the outer cask wall and in a vertical cut for a simplified CASTOR V/19 model. Right: Temperature difference between average cask wall temperature and ambient air temperature (20°C) over time.

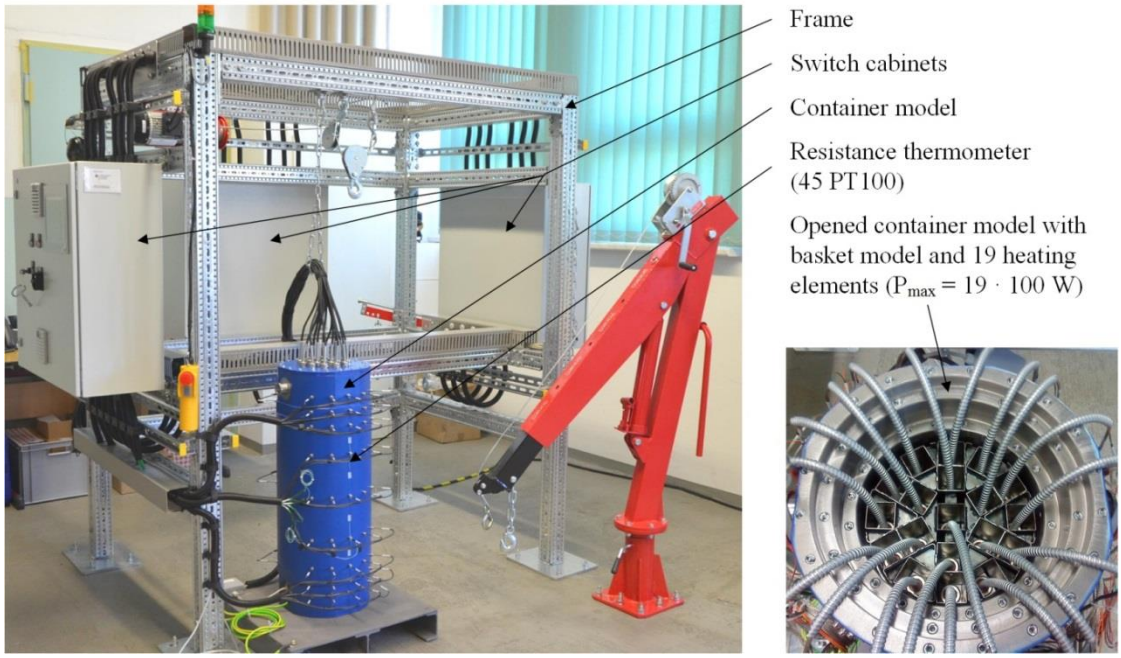

Fig. 2. Experimental rig for the investigations of the thermography method

3. Gamma and neutron radiation field

The measurement of external gamma and neutron radiation fields is probably the most conventional way to monitor sealed dry storage casks. This method, however, can be quite a challenge due to the massive shielding that is used to protect the environment from the radiation emitted from the fuel assemblies, as well as the self-shielding from the fuel assemblies themselves. For investigating the feasibility of using such a method to determine

the state of the fuel assemblies inside the cask, the gamma and neutron radiation fields outside the CASTOR V-19 with different fuel assembly states were simulated using the MCNP6 code [8]. The CASTOR V-19 design was modeled in detailed as shown in Fig. 3. The fuel assemblies inside the cask are again modelled as of a "Vor-Konvoi"-type German PWR with an average burnup of about 57 GWd/t. The fuel composition of the assemblies was extracted from a generic calculation of an equilibrium core with typical low-leakage loading. The gamma sources for the MCNP6 calculations were estimated using the FISPACT-II code [7]. The neutron sources, which are dominated by spontaneous fission and (α, n)-reactions, were estimated using the SOURCES-4C code [9]. The neutron and gamma radiation field was evaluated for a cask with all intact fuel assemblies and cask with one damaged or disfigured fuel assembly, mimicking a fuel assembly with clad ballooning and fuel relocation.

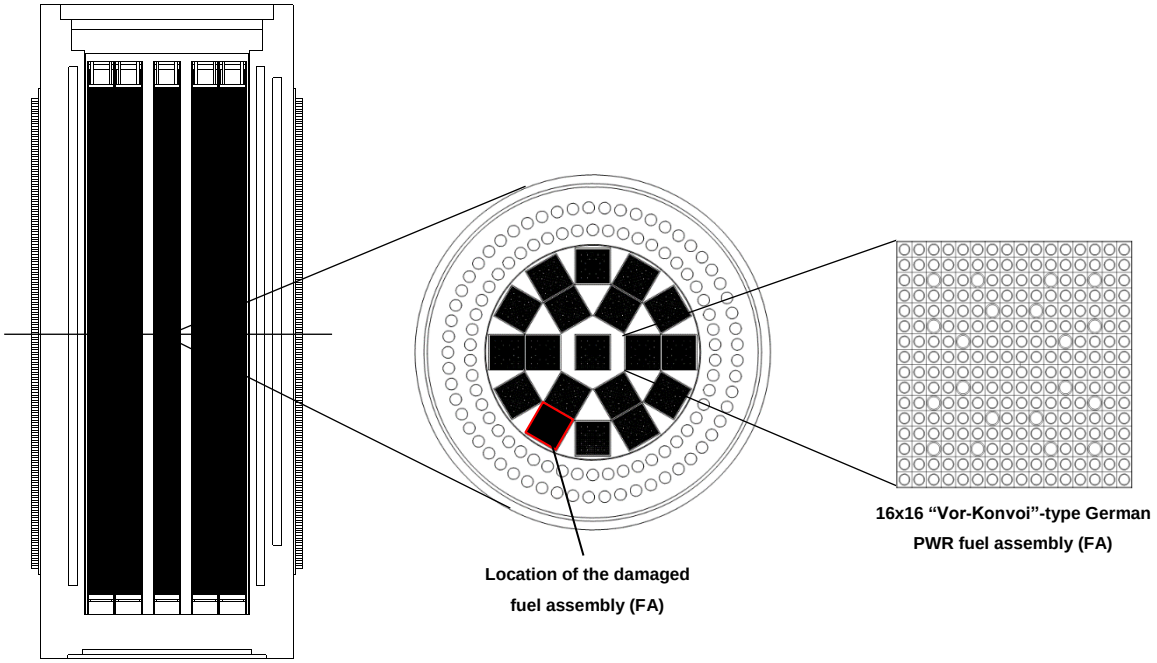

Fig. 3. MCNP model of a fully loaded cask

In general, the results of the investigation indicated that the more the damaged fuel assembly is close to the cask inner walls and that the damage is in a large scale, the more it can be detected by external radiation measurements. Fig. 4, for example, presents a comparison between the gamma radiation flux outside the sidewall of a cask with all intact fuel assemblies and a cask with one damaged fuel assembly. The gamma radiation flux was averaged in the azimuthal direction. The damaged fuel assembly was defined, in this case, as one with ballooned fuel rods. It was assumed that each fuel rod expanded uniformly along its axis by about 0.2 cm and as a result a fragmented fuel accumulated at the bottom of the rod (i.e., fuel relocation). The gamma source was evaluated here assuming five years cooling time. It should be noted that the damaged fuel assembly is located close to the inner sidewall of the cask (marked red in Fig. 3). In that case, the intensity and the shape of the gamma radiation flux are sufficient to distinguish between both of the cases. As can be noted from Fig. 5, there is a sharp reduction in the flux in the upper 30 cm of the fuel assembly's active

region ($462.415 \leq Z \leq 492.780$), adjacent to the location of the damaged fuel [10]. This reduction indicates the relocation of the fuel towards the bottom of the fuel rods.

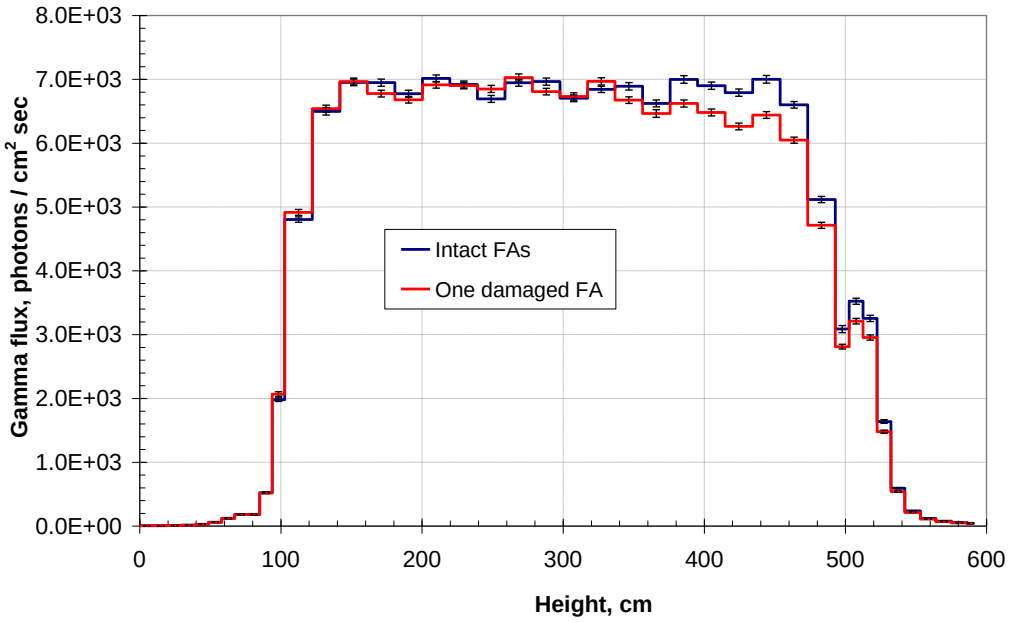

Fig. 4. Gamma flux outside the sidewall of the cask as a function of height

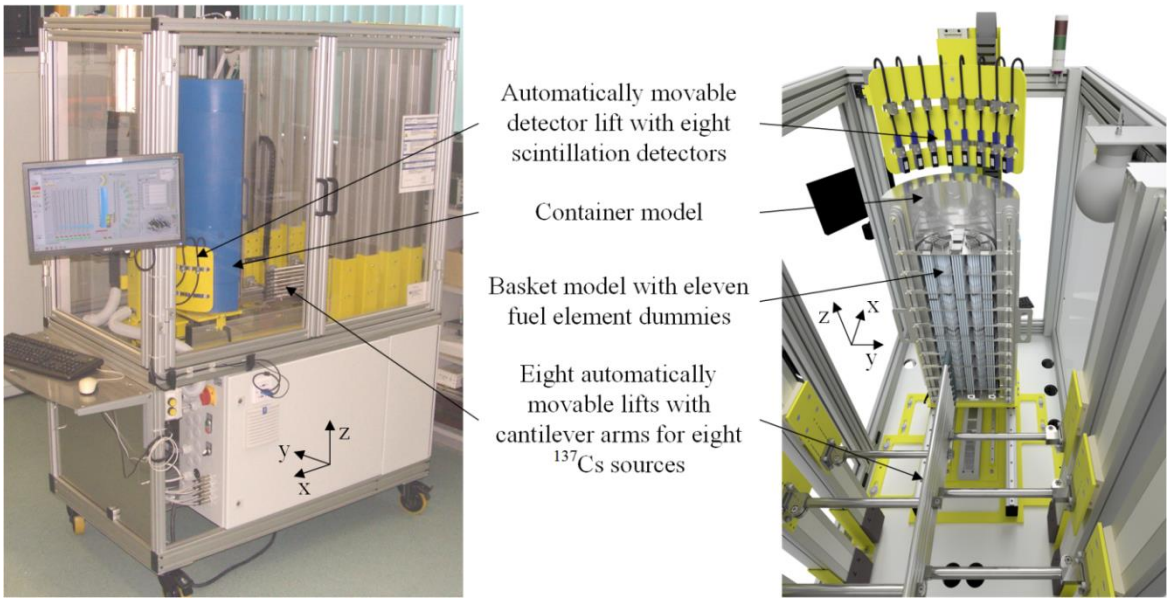

Fig. 5. Experimental rig for the investigations of the gamma flux measurements method

For further investigation of the external gamma flux measurements method and validation of the MCNP model setups described above, a cask-like experimental rig was constructed. The experimental rig consists of a halved, scaled (1:7.4) CASTOR V/19 model with integrated basket model, eleven fuel element dummies, eight ^{137}Cs sources, and eight scintillation detectors. The ^{137}Cs sources are attached on eight automatically movable lifts with cantilever arms. The scintillation detectors are radially arranged on an automatically

movable detector lift. Both, the sources and detectors, are movable in the vertical direction of the experimental rig. A view of the experimental rig is given in Fig. 5. The mobility of the ^{137}Cs sources allows generating a multitude of different gamma flux fields. Due to the cask and basket models as well as the eleven fuel element dummies (4 x 4 rods per dummy), which are fillable with metallic cylindrical pins, the generated gamma flux fields can be systematically changed. The scintillation detectors are used for the measurement of the resulting gamma flux fields outside of the cask model.

4. Cosmic muons

Cosmic-ray muons are elementary particles similar to electrons except with about 200 time's greater mass. Muons are produced from cosmic-ray collisions in the upper atmosphere and reach the earth at a flux of 10,000 $m^{-2}min^{-1}$ at sea level [11]. Muons are highly penetrating particles. The mean energy of muons at sea level is about 3-4 GeV, which is sufficient to penetrate meters of rock. Muons in the energy range of 0.1-1000 GeV interact with matter in two primary ways: energy loss through electromagnetic interaction with electrons resulting in ionization, and deflection via multiple Coulomb scattering from interactions with the matter nuclei. These two interactions underlie two different kinds of muon imaging techniques [12], namely muon transmission imaging, and muon scattering tomography imaging. The highly penetrating nature of the muon and the dependence of its interactions on material density make the muon imaging techniques an attractive idea for monitoring of sealed dry storage casks.

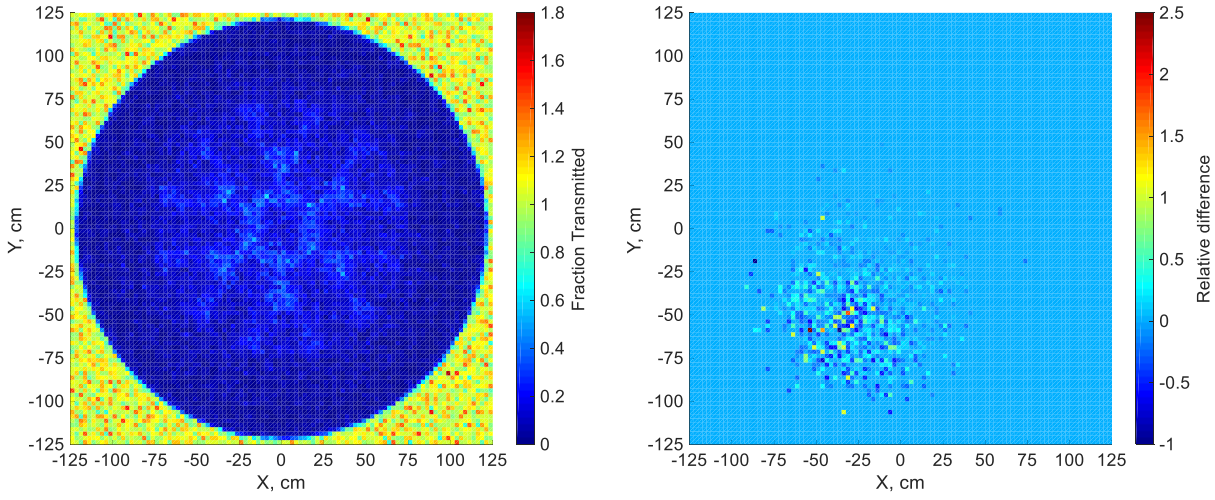

a) Fraction transmitted distribution **b) Relative difference distribution**

Fig. 6. Muon transmission imaging technique: a) muon fraction transmitted for a cask with one damaged fuel assembly, b) relative difference between a cask with one damaged fuel assembly and a cask with all intact fuel assemblies (reference case)

For studying the feasibility of using muon transmission imaging techniques for monitoring of the cask, the attenuated muon flux below the CASTOR V/19 with different fuel assembly states was evaluated using the MCNPX code [13]. The cask was modeled in detail as described in Section 3 and shown in Fig. 3. The muon source for the simulations was

generated over a plane of 10 m x 10 m located above the cask. A muon source with zenith angle of 0° and an energy spectrum corresponding to those of cosmic ray muons at sea level [14] was chosen for the study. The source was evenly distributed throughout the plane and was directed down towards the cask. Fig. 6a presents the muon fraction transmitted distribution for a cask with one damaged fuel assembly. The definition and the location of the damaged fuel assembly are the same as described in Section 3. Fig. 6b presents the relative difference distribution between this case and a cask with all intact fuel assemblies (reference case). As can be noted, although the image (Fig. 6b) is inherently blurred by the multiple scattering within the cask, the location of the damaged fuel assembly is quite visible.

By nature, muon transmission imaging provides a 2D image of the object. However, by combining several 2D projections, either by moving the muon detector around the object or by surrounding the object with several detectors, a 3D image can be achieved. Muon scattering tomography imaging, on the other hand, provides, by nature, 3D information about the object. It requires the placement of muon detectors on two opposite sides of the object. The detectors register the exact muon tracking information: muon track position and direction as they cross the detection planes. The muon tracking information is then used to reconstruct an image of the object using different reconstruction algorithms. Currently, within the frame of the project, a computer simulation code for objects reconstruction using muon scattering tomography imaging is underway.

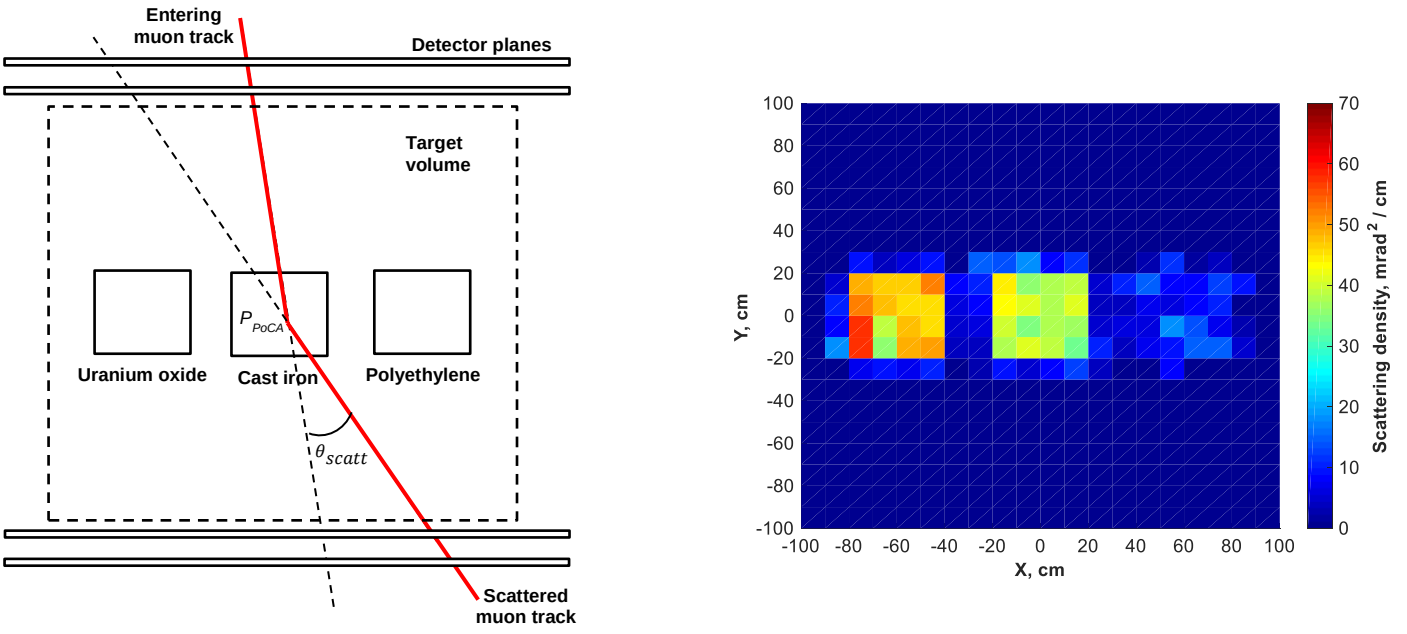

a) Schematic view of the PoCA algorithm test scenario

b) Scattering density distribution (from right to left: Uranium oxide, Cast iron, Polyethylene)

Fig. 7. Muon scattering tomography imaging technique: image reconstruction based on PoCA algorithm

As a first step in the computer simulation code development, the Point of Closest Approach (PoCA) reconstruction algorithm [15] was implemented and tested. When a muon

passes through a material, it undergoes a large number of deflections, mostly due to Coulomb scattering with nuclei of material. This effect is then called multiple Coulomb scattering. Muons are deflected more strongly by materials with high atomic numbers.

This mechanism provides a means of discriminating between low, medium and high-Z materials. PoCA is a heuristic algorithm originally designed as a proof of principle concept to show that muon scattering could be used to distinguish between low density, medium density, and high-density material. The test scenario used to evaluate the PoCA algorithm included three blocks (40 x 40 x 20 cm) made of Uranium oxide, Cast iron, and Polyethylene (structural materials of the CASTOR V/19), which represent high, medium, and low-density material. The blocks were placed horizontally (separated along with the x-plane) in the air between two muon detectors as shown schematically in Fig. 7a. The test scenario was simulated using the MCNPX code [16] to get the incoming and outgoing muon tracks. The muon source for the simulations was generated using the Cosmic-Ray Shower Generator (CRY) [17], which was coupled with the MCNPX code. The muon source was generated with an angular distribution and an energy spectrum corresponding to those of cosmic ray muons at sea level. The simulations were performed with 10 million muons generated over a plane of 10 m x 10 m. The obtained incoming and outgoing muon tracks information was used to reconstruct the blocks image using the PoCA algorithm. Fig. 7b presents the reconstructed image of the three blocks. As can be noted, it is possible to locate and distinguish between the different materials using the PoCA algorithm. This result provides interesting research lines for future investigation and continuous development. The future work is aimed at achieving a full comprehensive computer simulation code for imaging the interior of an object and in particular the cask using muon scattering tomography imaging.

5. Acoustic methods

Two methods of acoustical spectrometry are considered in this study for the monitoring of sealed dry storage casks. These two methods are:

- vibration analysis and
- sound emission analysis.

In vibration analysis, structure-borne vibrations are excited in the cask. The vibrations of the cask are then causing a vibration excitation of the basket and the fuel elements via the contact points. The vibrations of the basket and the fuel elements, in turn, influence the vibration behavior of the cask. The resulting vibration responses of the cask are measured by using suitable sensors. If vibration analyses are carried out for a cask at different times during the storage period (e.g., at the beginning of dry storage and frequently later), and the resulting vibration responses differ, a change in state of the cask or the inventory must have occurred.

For investigating applicability and sensitivity of the vibration analysis, the same experimental rig is used for investigations of the thermography method (Fig. 2). However, the heating elements are replaced by 19 fuel element dummies (16 rods per dummy, 4 x 4 arrangement), which are fillable with 464 metallic cylindrical pins (29 pins per rod) for a fuel replication. The 19 fuel element dummies give a comparable mass ratio between cask with basket and fuel elements as for a loaded CASTOR V/19. Vibrations are excited with an

impulse hammer with a force sensor, and the resulting responses are measured with a piezoelectric vibration transducer for acceleration measurement (Fig. 8, left).

For the experiments, four different states were defined and assessed. The first state (state 0) represents a cask filled with 19 intact fuel element dummies. The three remaining states (state 1-3) represent a cask filled with 18 intact fuel element dummies and one damaged fuel element dummy. In each of these cases, the damaged fuel element dummy was located at different places inside the cask, i.e. at center (position 1, state 1), at the inner fuel elements ring (position 2, state 2), and at the outer fuel elements ring (position 3, state 3). An intact fuel element dummy is defined as one with 29 pins in each rod. A damaged fuel element dummy is defined as one with 15 pins in each rod and 14 pins distributed between the rods in the bottom of the element. With that, the damaged fuel element dummy is mimicking an element with fuel relocation. It should be noted that the total mass remains the same for all of the defined states.

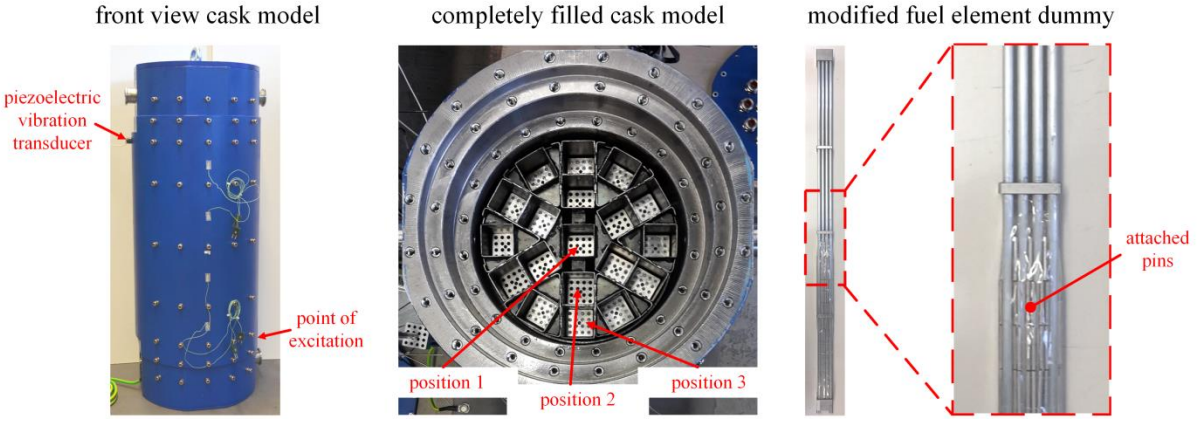

Fig. 8. Left: excitation and measurement points; central: completely filled cask model; right: modified fuel element dummy

For each of the four states, the acceleration-time signals were measured five times. Subsequently, each signal was transformed with the Fourier-Transformation into the frequency domain. As a result, 20 amplitude spectra for the four defined states were determined. The diagram in Fig. 9 shows exemplarily the amplitude spectra for each state. It can be seen that the amplitude spectra of all states are strongly similar and not classifiable by a human. The eigenfrequencies of the individual states are very close to each other.

Therefore, a computer-based classification of the amplitude spectra or different states is necessary. For that, an artificial neuronal network (type: multilayer perceptron) was developed. The development was performed with all of the 20 amplitude spectra for the four defined states (five amplitude spectra for each state). The developed artificial neuronal network was able to calculate integer state values between 0 and 3 for each of the 20 amplitude spectra. The results are shown in the diagram of Fig. 10. It can be seen that only for three amplitude spectra wrong state values were calculated by the artificial neuronal network. In particular, the artificial neuronal network was always able to distinguish the three damage states (states 1 till 3) from the normal state 0.

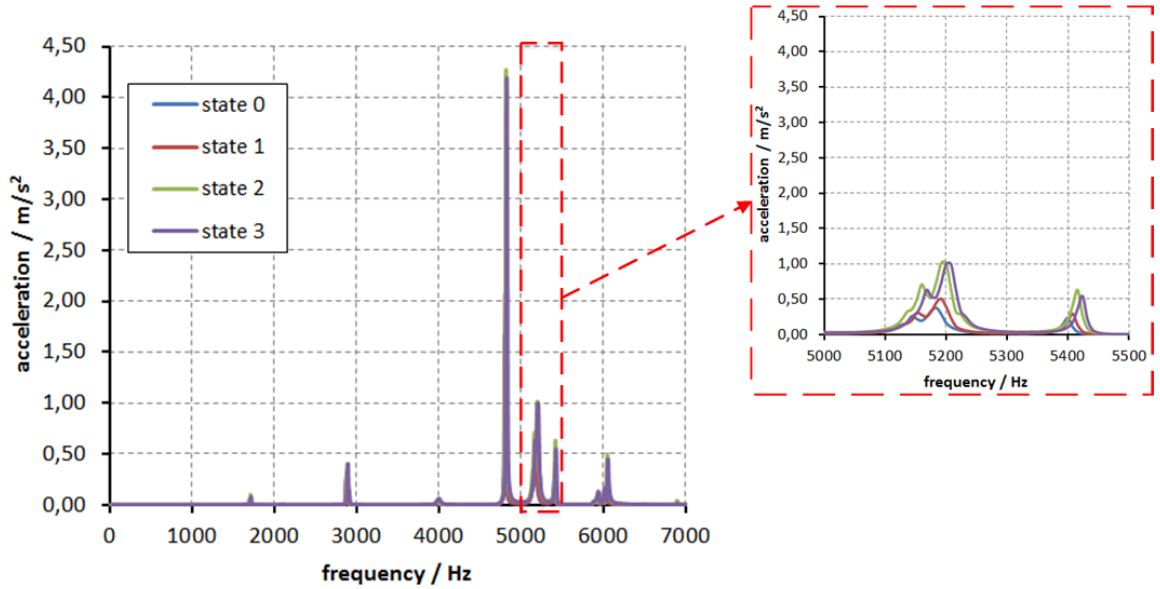

Fig. 9. Amplitude spectra of the first measurements for the four defined states

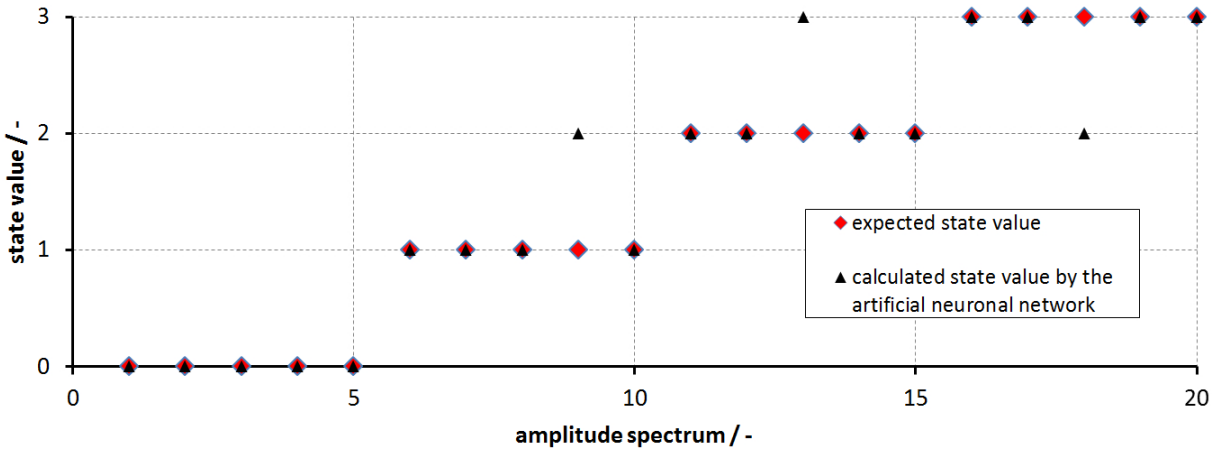

Fig. 10. Expected and by the artificial neural network calculated state values for the 20 amplitude spectra of the four defined states

The second method of acoustical spectrometry, namely the sound emission analysis, is aimed to detect ruptures of fuel rods during the time of dry storage and also the approximate position of a cask in which a fuel rod rupture happened. For that, a number of microphones have to be installed in an intermediate storage. In the case of a fuel rod rupture, the microphones will record the resulting sound waves, and with this a statement about the rupture is possible. Furthermore, run-times of acoustic signals will be analyzed to determine the position of the event in an intermediate storage.

In a first step, the sound level attenuation R through the cask wall was calculated, which was modeled as homogenous wall, by application of Heckl's fomula [18]:

$$R = \left(20 \lg \frac{\pi f m''}{\rho c} - 3\right) dB, \tag{1}$$

m'' mass per unit area / kg/m^2,
ρ air density / kg/m^3,
c speed of sound in air m/s.

For a frequency range from 0 to 1000 Hz, the attenuation is approximately 80 dB.

In a second step the rupture sound pressure level of a pre-damaged test rod (material: stainless steel, length: 600.0 mm, outer diameter: 10.0 mm, inner diameter: 8.4 mm), which has a similar characteristic to a real fuel rod cladding tube, was experimentally determined. For that the experimental rig was used, which is shown in Fig. 11. This consists mainly of a burst container, a compressor system, a heating element and various measuring devices (e. g. pyrometer, sound level meter, thermocouples, pressure sensor). The burst container and the peripheral components (pipelines, needle valves, etc.) are designed for test pressures up to maximum 1000.0 bar, test temperatures up to maximum 400.0 °C, as well as test volumes of 8.0 l (at 1000.0 bar; larger test volumes at lower test pressures possible). Test pressures up to 700.0 bar can be provided by the compressor system.

For the experiment the pre-damaged (radial removal of the outer diameter from 10.0 mm to 9.0 mm) test rod was clamped inside the container. The heating element (heated length: 570.0 mm, outer diameter: 8.0 mm) was inserted into the test rod. Subsequently, the pressure and temperature was increased inside the test rod up to the rupture point. With the sound level meter, which was positioned inside the container, the resulting sound emission was measured. The rupture point parameters were determined by a pyrometer (measuring temperature of outer test rod wall) and a pressure sensor.

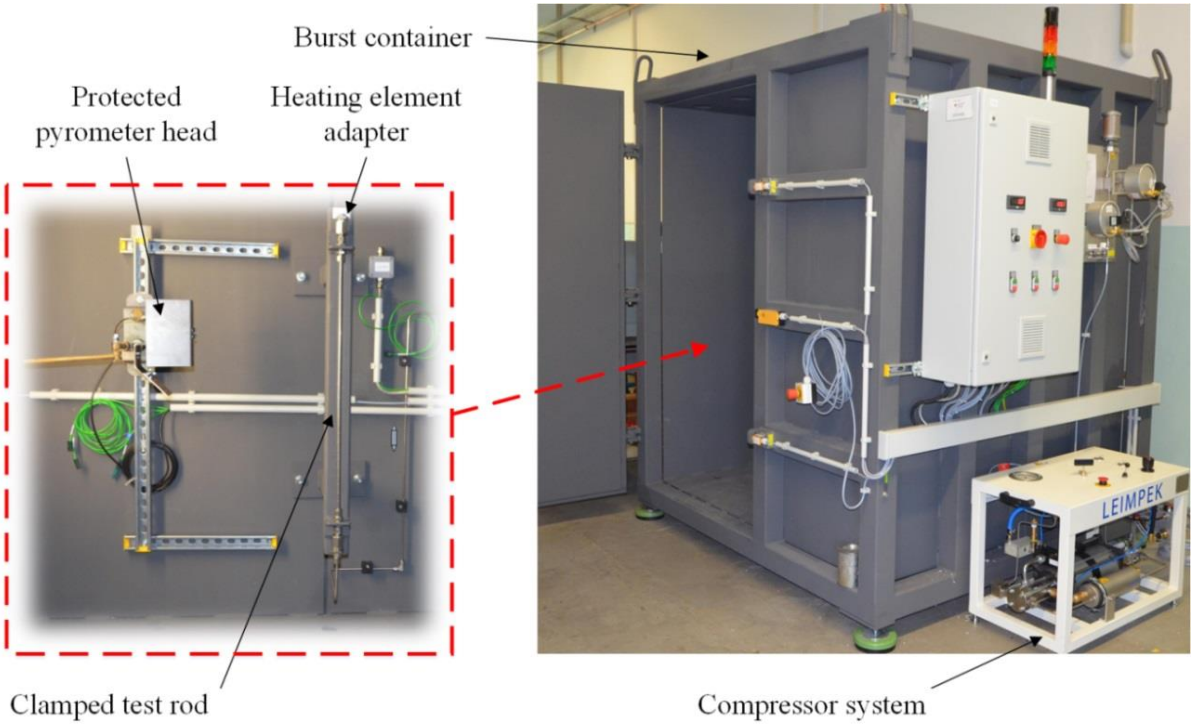

Fig. 11. Experimental rig for the investigations of the sound emission analysis method

As a result of the experiment, the test rod was ruptured in the pre-damaged area at an internal pressure of approx. 264.0 bar and a pipe temperature of approx. 136.0 °C. Though this pressure is somewhat higher than expected for prolonged intermediate storage period the experiments provide a first insight into the acoustics of rod rupture. The ruptured test rod is shown in Fig. 12. The maximum sound pressure level when rupturing the test rod was approx. 130 dB. Taking into account the determined sound level attenuation through a cask wall of

approximately 80 dB outside a real cask a sound pressure level of approximately 50 dB should be detectable. This corresponds approximately to the sound pressure level of a normal conversation. The investigations show that ruptures of fuel rods can be detected outside the dry storage cask.

In further investigations the rupture sounds of hydrogen embrittled Zr tubes are to be determined. Furthermore, the influence of extraneous noise in an intermediate storage on the detectability of ruptures sounds will be investigated.

Fig.12. Ruptured test rod

6. Conclusion and outlook

In this paper, we introduced potential methods to detect changes in the spent fuel inventory of dry storage casks. Due to the heavy construction of these casks, only a very limited number of methods are applicable. Such are thermography, radiation-based methods, and acoustic methods. We started the assessment of the applicability, sensitivity, and uncertainty of these methods using numerical and experimental techniques. All of the methods proved to have a fundamental capability of detecting severe changes of the fuel distribution inside the cask. Thermographic and radiation based methods rely on a significant relocation of fuel. Such may happen, if fuel rods balloon and embrittled fuel sacks down inside the rods or even runs out of the fuel rods due to cladding rupture. However, the degree of pulverization and the mobility of the fuel powder is still an open question. Acoustic methods are additionally sensitive to severe changes in the cladding structure.

The basic method assessment proved that each of the methods faces particular difficulties. Thermography is hampered by the complex convective heat transport inside the basket and the decreasing heating power over time. Methods based on gamma and neutron radiation have less predictability for the most internal fuel elements. Muon imaging requires expensive detectors and long data acquisition times. Acoustic emission needs a very subtle discrimination of small in-container signals from environmental noise, e.g., during decommissioning of power plants. For vibration spectroscopy, there are still open issues of sensitivity. Within the project, there is ongoing research activity to clarify the open points and eventually derive a suitable and validated approach for the long-term monitoring of extended dry storage of spent fuel.

Acknowledgment

This work was funded by the German Federal Ministry of Economic Affairs and Energy (BMWi) with the grant number 1501518A/B on the basis of a decision by the German Bundestag. Responsibility for the content of this report lies with the authors.

References

[1]. *Ellinger, A.; et al.:* Sicherheitstechnische Aspekte der langfristigen Zwischenlagerung von bestrahlten Brennelementen und verglasten HAW. GRS report (GRS-A-3597) to the project 3607R02599, (2010).

[2]. *Marchal, N.; Campos, C.; Garnier, C.:* Finite element simulation of Pellet-Cladding Interaction (PCI) in nuclear fuel rods. Computational Materials Science 45, pp. 821-826, (2009).

[3]. *Michel, B.; Sercombe, J.; Thouvenin, G.; Chatelet, R.:* 3D fuel cracking modelling in pellet cladding mechanical interaction. Engineering Fracture Mechanism 75, pp. 3581-3598, (2008).

[4]. *Wiesenack, W.:* Summary of the Halden Reactor Project LOCA Test Series IFA-650. Institutt for Energiteknikk, OECD Halden Reactor Project, Halden (Norwegen), Kurztitel: HPR-380, (2013).

[5]. *Klinger, R.:* Sicherheitsaspekte bei der längerfristigen Zwischenlagerung wärmeentwickelnder radioaktiver Abfälle. Presentation to the GRS expert talk, Berlin, (2015).

[6]. *Schrödl, E.; et al.:* Experimentelle Untersuchungen zum Verhalten von Brennstäben mit hohem Abbrand bei mechanischen Unfallbelastungen beim Transport. GRS report (GRS-A-3490) to the R&E project 3606R02558, (2010).

[7]. *Sublet, J. Ch., Eastwood, J. W., Morgan, J. G., Gilbert, M. R., Fleming, M., Arter, W.,* FISPACT-II: An Advanced Simulation System for Activation, Transmutation and Material Modelling, Nuclear Data Sheets, 139, 77-137 (2017).

[8]. *Goorley, T. et al.,* Initial MCNP6 release overview, Nucl. Technol., 180, 298-315 (2012.).

[9]. *W. B., Wilson, R. T., Perry, W. S., Charlton, T. A.,* Parish, Sources: A code for calculating (alpha, n), spontaneous fission, and delayed neutron sources and spectra, Progress in Nuclear Energy, 51, 608-613 (2009).

[10]. *R. Rachamin, U. Hampel*, "Feasibility Study for Detection of Fuel Assemblies State Inside Sealed Dry Storage Casks using External Gamma Flux Measurements", Proc. of 20th Topical Meeting of the Radiation Protection & Shielding Division of ANS, Santa Fe, NM, USA, August 26-31, 2018.

[11]. *K. Hagiwara, et al.,* Particle data group, review of particle physics, Phys. Rev. D 66 (1) (2002) 1.

[12]. *S. Procureur,* Muon imaging: Principles, technologies and applications, Nuclear Inst. and Methods in Physics Research, A 878, 169–179 (2018).

[13]. *G. W. McKinney et al.,* MCNPX 2.5.0 – New features demonstrated, Los Alamos National Lab., NM, Tech. Rep. LA-UR-04–8695 (2005).

[14]. *S. Haino et al.,* Measurements of primary and atmospheric cosmic-ray spectra with the BESS-TeV spectrometer. Physics Letters B, 594, 35-46 (2004).

[15]. *L.J. Schultz et al.,* Image reconstruction and material Z discrimination via cosmic ray muon radiography, Nuclear Instruments and Methods in Physics Research A, 519, 687–694 (2004).

[16]. *G. W. McKinney et al.,* MCNPX 2.5.0 – New features demonstrated, Los Alamos National Lab., NM, Tech. Rep. LA-UR-04–8695 (2005).

[17]. *C. Hagmann, D. Lange, and D. Wright*, Cosmic-ray shower generator (CRY) for Monte Carlo transport codes, Proc. of IEEE Nucl. Sci.Symp., Honolulu, HI, 2, 1143–1146 (2007).
[18]. *M. Heckl*, Die Schalldämmung von homogenen Einfachwänden endlicher Fläche, Acustica 10(2), pp. 98-108, (1960).

The authors of this contribution

Prof. Dr.-Ing. habil. Uwe HAMPEL
AREVA Endowed Chair of Imaging Techniques in Energy and Process Engineering, Technische Universität Dresden, 01062 Dresden, Germany, and
Helmholtz-Zentrum Dresden-Rossendorf, 01328 Dresden, Germany.
Tel. +49 351 260 3460
u.hampel@hzdr.de

Prof. Dr.-Ing. Alexander KRATZSCH
Zittau/Görlitz University of Applied Sciences, Institute of Process Technology, Process Automation and Measuring Technology, Theodor-Körner-Allee 16, 02763 Zittau, Germany
a.kratzsch@hszg.de

Dr. Reuven RACHAMIN
AREVA Endowed Chair of Imaging Techniques in Energy and Process Engineering, Technische Universität Dresden, 01062 Dresden, Germany.
r.rachamin@hzdr.de

Dipl.-Math. Michael WAGNER
AREVA Endowed Chair of Imaging Techniques in Energy and Process Engineering, Technische Universität Dresden, 01062 Dresden, Germany.
michael.wagner@hzdr.de

M. Eng. Sebastian SCHMIDT
Zittau/Görlitz University of Applied Sciences, Institute of Process Technology, Process Automation and Measuring Technology, Theodor-Körner-Allee 16, 02763 Zittau, Germany
s.schmidt@hszg.de

Dipl.-Ing. (FH) Daniel FIß
Zittau/Görlitz University of Applied Sciences, Institute of Process Technology, Process Automation and Measuring Technology, Theodor-Körner-Allee 16, 02763 Zittau, Germany
d.fiss@hszg.de

Dipl.-Ing. (FH) Sebastian REINICKE
Zittau/Görlitz University of Applied Sciences, Institute of Process Technology, Process Automation and Measuring Technology, Theodor-Körner-Allee 16, 02763 Zittau, Germany
s.reinicke@hszg.de